THE JOURNAL OF PHYSICAL CHEMISTRY B

Article

pubs.acs.org/JPCB

Time-Resolved Infrared Absorption Studies of the Solvent-Dependent Photochemistry of ClNO

Joshua D. Patterson and Philip J. Reid*

Department of Chemistry, University of Washington, Box 351700, Seattle, Washington 98195, United States

ABSTRACT: The photochemistry of nitrosyl chloride (ClNO) dissolved in cyclohexane is investigated using ultrafast time-resolved infrared (TRIR) spectroscopy. Following 266 nm photolysis, the photochemistry is measured by following changes in optical density at frequencies spanning the N=O stretch fundamental transition. A photoinduced depletion in optical density is observed consistent with the depletion of ground-state ClNO. The depletion in optical density remains constant out to ~50 ps demonstrating that ClNO photodissociation is not followed by recombination of the Cl and NO photofragments. In addition, no evidence for the formation of the ClON photoisomer is observed. These results stand in contrast to previous studies in acetonitrile where ClNO photolysis is followed by geminate recombination of Cl and NO, and by the production of ClON. These differences in ClNO photochemistry are proposed to arise from the population of different excited-states caused by solvent dependence of the ground-state potential energy surface minimum along the Cl−N stretch coordinate. Solvent-dependent vibrational relaxation and differences in strength of the solvent cage are also proposed to contribute to the solvent-dependent photochemistry. Finally, these results are placed in the context of recent models of ClNO photochemistry and role of this compound in tropospheric ozone production.

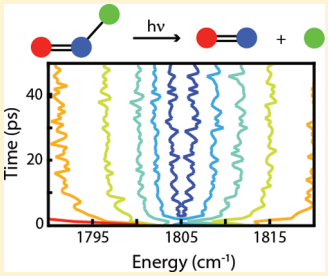

INTRODUCTION

Sunlight is a central component in a variety of atmospheric chemical processes and is responsible for the production of reactive species in both the troposphere and stratosphere.[1] The heterogeneous nature of the atmosphere including the variation in environment (surfaces, aerosols, droplets, etc.) adds to the complexity of this chemistry. A first step in understanding the role of phase in atmospheric photochemistry is to examine the reactivity of atmospherically relevant species over a range of well-defined environments to determine which properties of the environment influence the photochemistry of interest. For example, the photochemistry of chloride dioxide (OClO) is remarkably phase dependent. Photoexcitation of gaseous OClO results exclusively in formation of OCl and O.[2−4] In contrast, excitation of OClO in low-temperature matrixes results in the formation of the photoisomer, ClOO.[5−7] The photochemistry in solution exhibits intermediate behavior, where ClO/O, Cl/O_2, and ClOO production are all observed.[8−18] The chemistry of OClO illustrates that changes in environment can significantly impact photochemistry.[19]

To further explore the phase-dependent photochemistry of atmospherically relevant compounds, we have investigated the reaction dynamics of nitrosyl chloride (ClNO). Stratospheric ClNO is formed by the reaction of HONO on frozen HCl surfaces, while tropospheric production proceeds through the reaction of NO_2 with airborne NaCl from sea spray.[20] Recent studies have suggested a new ClNO formation pathway where HCl reacts with surface bound NO_2 to produce ClNO.[21] Inclusion of this pathway into current tropospheric models resulted in an 8 ppb increase in ClNO mixing ratios in the South Coast Air Basin, suggesting that ClNO significantly impacts the oxidative potential of the troposphere.

Given the diversity of environments in which ClNO is produced, understanding the environmental-dependence of ClNO photochemistry is important in evaluating its impact on atmospheric processes. The evidence to date suggests that the photochemistry of ClNO is remarkably sensitive to environment. Resonance Raman (RR) studies established that the frequencies of the N−Cl stretch (ν_2) and bend (ν_3) transitions are solvent dependent, shifting to lower frequency in more polar solvents.[22] Fourier transform infrared (FTIR) absorption studies of the N=O stretch (ν_1) fundamental transition observed that this transition shifts to higher frequency and the line width increases with an increase in solvent polarity.[23] The influence of solvent in ClNO photochemistry was investigated using femtosecond pump−probe spectroscopy.[24] Experiments in acetonitrile and chloroform observed the photoinduced depletion of ground-state ClNO followed by the production of Cl and NO in both solvents. In addition, these studies provided evidence for the formation of the photoisomer, ClON. Partial recovery in optical density associated with the photoinduced depletion of ground-state ClNO was observed with time constants of 3.7 ± 1.0 ps and 7.9 ± 1.0 ps in acetonitrile and chloroform, respectively. These results demonstrate that the photoproduct formation and geminate recombination dynamics are solvent dependent. Recent time-resolved infrared (TRIR) studies have also explored the photochemisty of ClNO in acetonitrile. Here, the evolution in optical density in the region of the ν_1 transition of ClNO was measured following 266 nm

Special Issue: Richard A. Mathies Festschrift

Received: December 5, 2011
Revised: February 22, 2012
Published: March 6, 2012

dx.doi.org/10.1021/jp211697r | J. Phys. Chem. B 2012, 116, 10437−10443

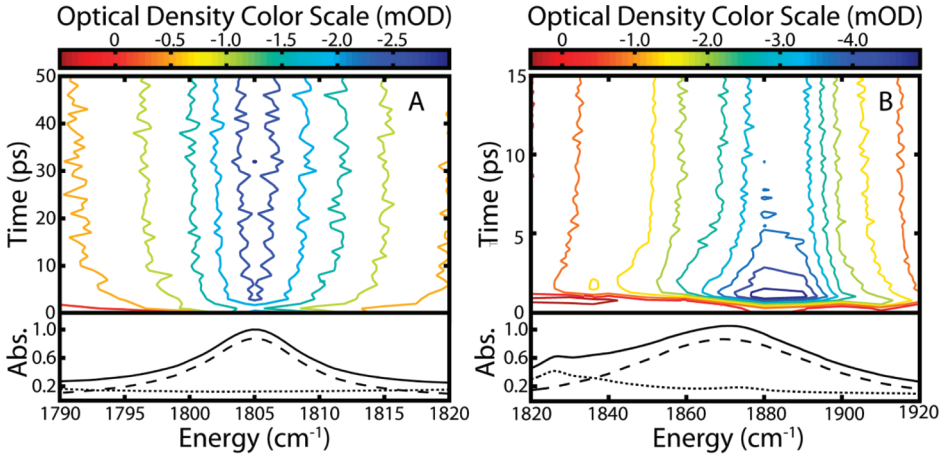

Figure 1. Contour plots of the photoinduced evolution in optical density observed in the spectral region of the NO-stretch fundamental transition for (A) ClNO dissolved in cyclohexane and (B) ClNO dissolved in acetonitrile. The change in optical density is indicated by the contour lines, the color scales provide a measure of the absolute optical density change. The FTIR absorption spectra of (A) ClNO in cyclohexane (solid), cyclohexane only (short dashed), and NO-stretch of ClNO (long dash) and (B) ClNO in acetonitrile (solid), acetonitrile only (short dashed), and NO-stretch of ClNO (long dash) are displayed in the lower panel.

photoexcitation.[23] Photoinduced depletion of ground-state ClNO and subsequent geminate recombination of the primary photofragments resulting in ClNO reformation was measured with a quantum yield of 0.54 ± 0.06. A transition at 1860 cm^{-1} assigned to ClON was also observed with an estimated production quantum yield of 0.07 ± 0.02.

In this article, we present TRIR studies of ClNO dissolved in cyclohexane. Photoexcitation at 266 nm results in long-time depletion of ground-state ClNO with no evidence of geminate recombination of the primary Cl and NO photofragments. In addition, the formation of the ClON photoisomer is not observed. A positive optical density offset is observed at 1870 cm^{-1} consistent with the production of NO. These results demonstrate that ClNO photoexcitation in cyclohexane results exclusively in production of Cl and NO. These results stand in contrast to the photochemistry observed in acetonitrile where geminate recombination and ClON production are both observed. We propose that solvent-dependence of the potential energy surface energetics, the strength of the solvent cage, and variation of the vibrational relaxation rate are responsible for differences in ClNO photochemistry observed between cyclohexane and acetonitrile. Finally, the implications of these results on recent models of ClNO tropospheric photochemistry are discussed.

EXPERIMENTAL SECTION

The apparatus employed in these studies has been described in detail elsewhere.[23] A Ti:Sapphire oscillater (KM Laboratories) was pumped by the frequency doubled output of a Nd:YVO_4 laser (Spectra Physics Millennia V), and the oscillator output was used to seed a Ti:Sapphire regenerative amplifier (Spectra Physics Spitfire) to produced 35 fs pulses (full-width at half-maximum) centered at 800 nm with an energy of 1 mJ/pulse at 1 kHz. The amplifier output was split using a 60/40 beamsplitter, and the higher-energy beam was used to pump an optical parametric amplifier (OPA, Quantronix TOPAS). Signal and idler fields at 1397 and 1868 nm, respectively, were overlapped in a $AgGaS_2$ crystal (Type I) for difference frequency generation (DFG) to produce the 5.55 μm probe field with a pulse energy of 1 μJ. The lower-energy portion of the amplifier output was passed through a pair of SF10 prisms to compensate for group-velocity dispersion and then frequency tripled with series of β-BBO crystals (types I and II) to generate the 266 nm pump field. Temporal delay of the pump relative to the probe was achieved by delivering the pump to a retroreflector mounted on a motorized delay stage (Newport ES300). The polarization of the pump field was set to 54.7° relative to the probe using a zero-order half-wave plate to minimize contributions from rotational dynamics to the optical-density evolution. The pump field (3 μJ/pulse) was weakly focused to a 1 mm diameter spot on the sample. The probe field was collimated using a pair of off-axis parabolic mirrors and then passed through a 50/50 CaF_2 beamsplitter with the reflected and transmitted beams serving as signal and reference beams, respectively. The signal beam was focused on the sample using an off-axis parabolic mirror. Spatial and temporal overlap of the pump and probe fields was established using the change in optical density in a Si wafer following 266 nm photoexcitation. This method was used to establish the 250 ± 50 fs time resolution of the apparatus.

After passing through the sample, the signal was collimated and delivered to a 0.25 m single-stage spectrograph (Jarrell Ash) equipped with a 100 groove/mm grating (λ_{blaze} = 5.6 μm) to isolate individual frequency components of the probe field with a resolution of 4 cm^{-1}. The reference beam was passed through the spectrograph displaced vertically from the signal. The signal and reference were focused onto a pair of LN_2 cooled MCT detectors (Infrared Associates). Detector outputs were delivered to gated integrators, and the integrator outputs were subtracted on a shot-to-shot basis. A mechanical chopper, operating at 500 Hz, was placed in the pump field to block every other pump pulse. Successive probe signals were subtracted from each other to determine the pump-induced change in optical density. Each time point was averaged over 5000 laser shots, with each measurement consisting of the average of 5 time traces.

The synthesis of ClNO has been described elsewhere.[22,23,25] Briefly, 8.75 g of sodium nitrite (Mallinckrodt Chemicals, 97.0%) was dissolved in 12.5 mL of H_2O and added dropwise to 50 mL of concentrated HCl (J. T. Baker, 37.6%). The solution was stirred, and the resulting ClNO gas was bubbled into a chilled flask containing cyclohexane (EMD OmniSolv,

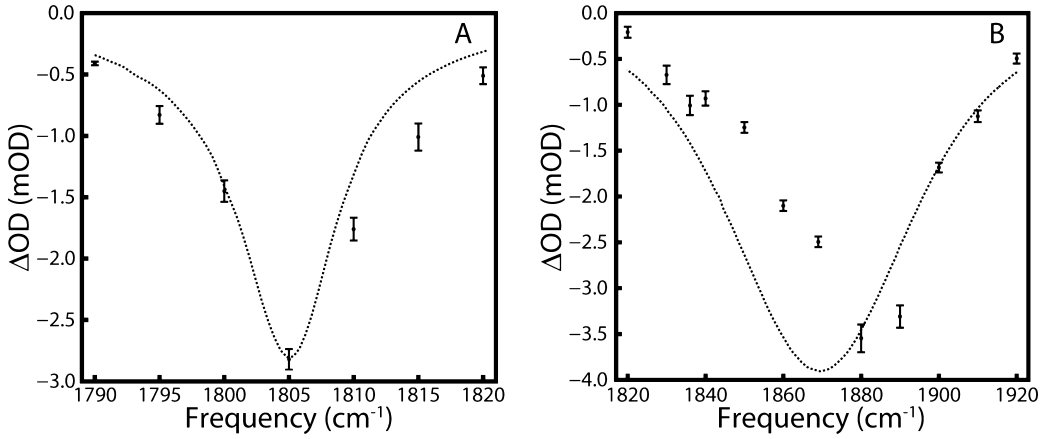

Figure 2. Long-time optical density offsets in the region of the NO-stretch fundamental transition of (A) ClNO dissolved in cyclohexane and (B) ClNO dissolved in acetonitrile. The points represent the experimental data with the associated error bars. The dashed lines indicate the band shape of ClNO in cyclohexane (A) and acetonitrile (B). The experimental data matches the band shape in cyclohexane indicating that the observed dynamics correspond to ground-state bleach of ClNO. The experimental data does not match the band shape in acetonitrile indicating the presence of an underlying absorptive feature assigned to the isomer, ClON.

99.91%). The sample was delivered to a Teflon flow cell (Harrick Scientific, 500 μm path length) equipped with BaF_2 windows. Sample concentrations, adjusted between 50 and 60 mM, were verified using UV−vis absorption. To prevent the degassing of ClNO from solution, sample bottles were placed in a temperature-controlled water bath set to 20 °C and sealed with a cap equipped with throughput compression fittings.

RESULTS

TRIR Studies of ClNO in Solution. The evolution in optical density following ClNO photoexcitation in cyclohexane is presented as a two-dimensional contour plot in Figure 1A. The FTIR absorption spectrum of ClNO dissolved in cyclohexane and individual contributions from ClNO and cyclohexane are presented in the lower panel of Figure 1A. The frequency region investigated in this study is dominated by the N═O stretch fundamental transition (ν_1) centered at 1805 cm^{-1}. No underlying transitions associated with the solvent are evident in this spectral region. The figure illustrates that following ClNO photoexcitation, a decrease in optical density is observed over the entire breadth of the N═O stretch (1790 to 1820 cm^{-1}) consistent with the depletion of ground-state ClNO. The initial depletion remains constant in magnitude out to the longest time investigated (50 ps), with a maximum depletion of 2.82 mOD measured at the peak of the ν_1 transition. To check that the depletion in optical density observed in cyclohexane arises exclusively from a decrease in intensity of the N═O stretch, the change in optical-density measured to the longest time delay is compared to the band shape of the N═O stretch in Figure 2A. The agreement between the optical-density depletion and the N═O stretch band shape evident in the figure demonstrates that the optical-density evolution observed in this solvent is due exclusively to the photodepletion of ground-state ClNO.

Figure 1 demonstrates that optical-density evolution observed following ClNO photolysis in cyclohexane is remarkably different than that observed in acetonitrile. First, the N═O stretch fundamental transition in acetonitrile is significantly broader (55 cm^{-1} fwhm in acetonitrile compared to 11 cm^{-1} in cyclohexane) and shifted to higher frequency (1869 cm^{-1} in acetonitrile versus 1805 cm^{-1} in cyclohexane). Next, in both solvents, a decrease in optical density is observed corresponding to the photoinduced depletion of ground-state ClNO. In cyclohexane, this depletion remains constant to the longest delays, but in acetonitrile, the initial depletion partially recovers with an increase in delay time consistent with geminate recombination resulting in the reformation of ground-state ClNO. As reported previously, detailed analysis of the optical density evolution established that the geminate recombination quantum yield in acetonitrile is 0.54 ± 0.06.[23] The results presented in Figure 1 demonstrate that geminate recombination of the primary photofragments does not occur in cyclohexane. Also in contrast to cyclohexane, the maximum reduction in optical density in acetonitrile occurs at 1880 cm^{-1} shifted from the maximum of the ν_1 transition at 1869 cm^{-1}. The long-time change in optical-density observed in acetonitrile (Figure 1B) is compared to the band shape of the N═O stretch in Figure 2B. The difference between these two spectra stands in contrast to the agreement observed in cyclohexane (Figure 2A) and suggests that something other than the depletion of ClNO is contributing to the optical-density evolution observed in aceontrile. Previous analysis of these results demonstrated that the photoisomer, ClON, also contributes to the optical-density in this spectral region, with quantitative analysis of the optical-density changes establishing that the quantum yield for ClON formation in acetonitrile is 0.07 ± 0.02.

Photoproduct Identification. A continually vexing problem in condensed-phase photochemistry is identifying the products that are formed following photolysis. Typically, gas phase and solid matrix spectroscopic data are employed to infer photoproduct spectroscopic signatures in solution. For ClNO, the vibrational transitions in cyclohexane are remarkably similar to those observed in argon matrixes. Specifically, the fundamental vibrational transitions for the N═O stretch, N−Cl stretch, and bend in argon are at 1804.8, 585.2, and 321.1 cm^{-1}, respectively.[26,27] Resonance Raman spectra of ClNO dissolved in cyclohexane place the fundamental transition of the N−Cl stretch and bend at 585 and 325 cm^{-1}, similar to the low-temperature argon data.[22] Furthermore, the N═O stretch fundamental was observed at 1805 cm^{-1} in cyclohexane using FTIR.[23] The similarities of transition frequencies between cyclohexane and argon matrixes suggest that the photoproduct vibrational frequencies in argon provide a reasonable guide as

to their location in cyclohexane. The N=O stretch fundamental transition of the photoisomer, ClON, is located at 1842 cm^{-1} in low-temperature argon.[26,27] In addition, several studies have identified the N=O stretch of free NO at 1875 cm^{-1} in argon.[28,29] If these transitions appear at similar frequencies in cyclohexane, then the vibrational signatures from these photoproducts should be resolvable in our experiment.

Figure 3 presents the temporal evolution in optical density measured at 1840 and 1870 cm^{-1} resonant with the expected

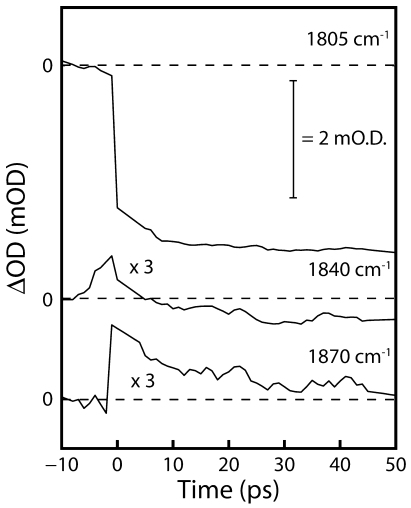

Figure 3. Evolution in optical density following photoexcitation at 266 nm of ClNO dissolved in cyclohexane. Probe frequencies 1805, 1840, and 1870 cm^{-1} are associated with the NO-stretch fundamental transitions of ClNO, ClON, and NO, respectively. Time traces at 1840 and 1870 cm^{-1} have been magnified by a factor of 3 for clarity.

N=O stretch of ClON and NO, respectively. For comparison, the photoinduced depletion of ground-state ClNO measured at 1805 cm^{-1} is also presented. Evaluation of the dynamics from 0 to 20 ps is complicated by a small contribution from the windows of the sample cell; however, the magnitude of the optical density offsets at longer delays are unaffected by this contribution and can be used to place estimates on the extent of ClON and NO formation. Using Beer's Law and the molar extinction coefficient of the N=O stretch, the long-time optical density offset at 1805 cm^{-1} is 2.82 ± 0.08 mOD corresponding to 0.038 mM of ClNO being photoexcited.[23] Previous studies have shown that the IR extinction coefficient of ClON is 4 ± 0.5 times greater than that of ClNO.[26] If all photolyzed ClNO was converted to ClON, a corresponding increase of ~11.28 mOD would be observed at 1840 cm^{-1}. In contrast, there is essentially no optical density increase observed at 1840 cm^{-1} at the longest delay times (Figure 3). Previous work in acetonitrile established the quantum yield for ClON production to be 0.07 ± 0.02.[23] If the quantum yield for ClON production is the same in cyclohexane, then the increase in optical density at 1840 cm^{-1} should be ~0.07 mOD, which is also significantly greater than what is observed. In short, the evolution in optical density at 1840 cm^{-1} (Figure 3) demonstrates that ClON is not a photoproduct of ClNO in cyclohexane.

Recently, the IR absorption of NO following photolysis of sodium nitroprusside in methanol was observed at 1851 cm^{-1} with a 23 cm^{-1} fwhm line width and an integrated area of 1.7 × 10^2 M^{-1} cm^{-2}.[30] Assuming similar oscillator strength in cyclohexane, the molar extinction coefficient of NO at 1870 cm^{-1} is predicted to be ~7 M^{-1} cm^{-1}. If all depleted ClNO is converted to Cl + NO, the resulting increase in optical density at 1870 cm^{-1} is estimated to be 0.013 mOD. This estimate is in surprisingly good agreement with 0.02 mOD long-time increase in optical density measured at 1870 cm^{-1} (Figure 3). The observed positive optical density offset at 1870 cm^{-1} combined with the absence of signal at 1840 cm^{-1} is consistent with the exclusive production of Cl + NO following ClNO photoexcitation in cyclohexane.

DISCUSSION

The results presented here demonstrate that the solvent can have a pronounced impact on photoproduct formation and geminate recombination in ClNO photochemistry. A variety of solvent and solute properties can influence this photochemistry including solvent−solute and solute−solute intermolecular interactions, solvent cage strength, and vibrational lifetime/coupling between the solute and solvent. We explore the role of each of these properties with regards to ClNO photochemistry below.

Solvent Cage Strength. The results presented above demonstrate that geminate recombination of the primary photofragments resulting in ground-state ClNO production does not occur in cyclohexane and occurs on short time scales (~5 ps) in acetonitrile consistent with the photofragments being confined to the first solvent shell or the solvent cage before recombination.[31−34] A possible explanation for the solvent dependence of the geminate recombination quantum yield is the existence of a stronger solvent cage in acetonitrile relative to cyclohexane, with the strength of the cage determined by the strength of the intermolecular interactions between solvent molecules. In cyclohexane, van der Waals forces are responsible for association, while stronger dipole−dipole interactions are operative in acetonitrile. Therefore, we would expect the geminate recombination quantum yield to be greater in acetonitrile relative to cyclohexane, as observed for ClNO. However, this result is not universal. For example, the observed 0.13 reduction in geminate recombination quantum yield for OClO in D_2O relative to H_2O suggests that solvent cage strength is not the only factor dictating the extent of geminate recombination.[19] Therefore, the increased quantum yield for geminate recombination in acetonitrile relative to cyclohexane suggests that the strength of the solvent cage is only one factor influencing the ClNO geminate recombination quantum yield.

Solvent Polarity and State Energetics. Previous studies have shown that the ground-state structure of ClNO depends on solvent polarity. Specifically, the frequency of the bend and N−Cl stretch fundamental transitions shift from 325 and 585 cm^{-1} in cyclohexane to 310 and 545 cm^{-1} in acetonitrile, respectively.[22] In addition, the N=O stretch shifts from 1805 cm^{-1} in cyclohexane to 1869 cm^{-1} in acetonitrile.[23] These shifts have been proposed to arise from the unique bonding structure of ClNO where the N−Cl bond is created by the weak overlap of a Cl p orbital and a singly occupied 2π antibonding orbital of NO.[35] Increasing solvent polarity shifts electron density from the NO antibonding orbital to the Cl p orbital thereby strengthening the NO bond and weakening the N−Cl bond. The dependence of ClNO structure on solvent is reflected in the absorbance spectrum of ClNO with the peak of the A-band shifting from 206 nm in cyclohexane to 218 nm in acetonitrile.[22] Using resonance Raman intensity analysis

dx.doi.org/10.1021/jp211697r | J. Phys. Chem. B 2012, 116, 10437−10443

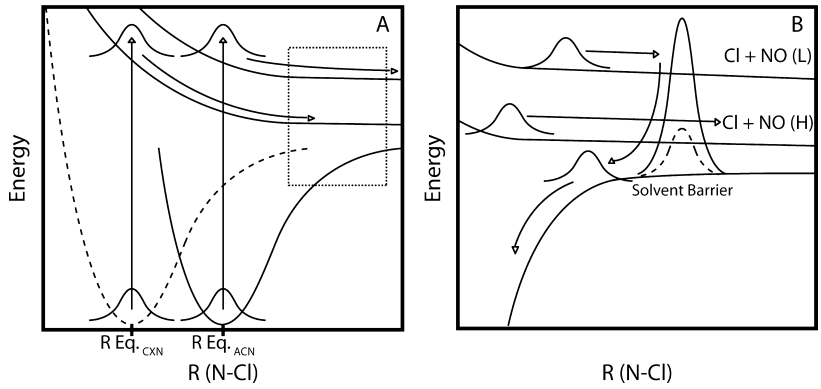

Figure 4. (A) Schematic of excited-state evolution along the reaction coordinate following photoexcitation at 266 nm. The ground-state potential of ClNO in cyclohexane (long dash) and acetonitrile (solid) shifts to longer equilibrium N−Cl bond distance with increasing solvent polarity allowing for different excited-state access with fixed excitation energy. (B) Excited-state evolution at large displacements along the reaction coordinate. Excitation of ClNO in acetonitrile populates an excited-state corresponding to Cl + NO production with low translational excitation (L). Lacking sufficient energy to cross the acetonitrile solvent barrier (solid line), excited ClNO relaxes back to the ground-state resulting in geminate recombination. Excitation in cyclohexane populates a state that results in Cl + NO with high translational energy (H) imparted to the photofragments allowing them to surmount the cyclohexane solvent barrier (long dash).

(RRIA), Nyholm and Reid demonstrated that this shift was consistent with displacement of the ground-state potential energy surface minimum to larger displacements along the N−Cl stretch coordinate. Altering the position of the ground-state potential relative to the excited-state could impact which transitions are accessed for a given excitation energy and could subsequently be responsible for the solvent-dependence observed in ClNO photochemistry.

Numerous gas-phase photochemical studies of ClNO have speculated on the nature of the excited-states accessed with A-band photoexcitation. Following A-band photoexcitation of gaseous ClNO, dissociation to form Cl and NO occurs. With 197 nm excitation, the NO photofragment is produced with vibrational excitation up to $n = 11$.[36] Further studies observed that the extent of NO vibrational excitation increases with increasing photolysis energy.[37,38] Time-of-flight analysis using 193 nm excitation revealed a bimodal vibrational state distribution of the NO fragment, with one component associated with NO populating vibrational states $n = 0$ to 24, and the other $n = 12$ to 20.[39] This result was interpreted in terms of the A-band arising from two different excited-states that correlate with two distinct dissociation channels. With regards to Cl production, both $Cl(^2P_{3/2})$ and $Cl^*(^2P_{1/2})$ have been observed following 236 nm excitation supporting the two state A-band model.[40] Felder and Morley, using photofragment translational energy spectroscopy, proposed that the A-band may consist of three states rather than two, assigning the transitions and their associated states in order of decreasing oscillator strength as, A_c ($S_5(4^1A') \leftarrow S_0(1^1A')$), A_b ($S_4(3^1A') \leftarrow S_0(1^1A')$), and A_a $T_5(3^3A') \leftarrow S_0(1^1A')$). Population of the A_c and A_b states was proposed to result in the production of vibrationally excited NO, while population of the A_a state results in the production of vibrationally cold NO with high translational excitation.[41] Skorokhodov et al. examined Cl*/Cl photoproduct branching ratios following 235 nm excitation and observed low and high translational energy components in both Cl* and Cl distributions.[42] High translational components maintained a 1:1 Cl*/Cl branching ratio and accounted for 37% of the observed total Cl production, while the lower energy component accounted for 63% and a 1:4 Cl*/Cl. These results were interpreted in terms of an avoided crossing leading to partitioning between high and low photofragment translational energy pathways. Solution phase studies of ClNO have also attempted to resolve the nature of the A-band. Resonance Raman depolarization ratios for ClNO were measured to be $\neq 1/3$ consistent with the A-band being composed of a minimum of two electronic transitions.[22] The resonance Raman and absorption cross-sections were successfully reproduced using two excited-states, confirming the existence of multiple states within the A-band.

We propose that a contributing factor to the solvent-dependence of ClNO photochemistry is that different excited-states are accessed in cyclohexane relative to acetonitrile. As discussed earlier, resonance Raman and FTIR studies have noted large frequency shifts with changes in solvent environment, indicating that the ground-state structure of ClNO is modified by solvent polarity.[22,23] RRIA studies determined that the excited-state slope decreased between cyclohexane and acetonitrile supporting variation in the excited-states populated by A-band excitation in different solvents. If we compare the solvent-dependent shift in the location of the A-band relative to its location in the gas phase, in cyclohexane, 266 nm photolysis would be equivalent to 256 nm excitation in the gas phase. As described earlier, 256 nm excitation results in population of the weak spin-forbidden A_a transition leading to the production of vibrationally cold NO with high translational excitation.[42] If this same photochemical channel is accessed in cyclohexane, then the high translational energy of the photofragments would provide for reduced geminate recombination. In acetonitrile, 266 nm photolysis would be equivalent to 244 nm excitation in the gas phase. Gas phase studies with 248 nm excitation have observed bimodal distributions of internal energies of the NO photofragments consistent with partitioning in accessing the A_a and A_b states. Access to both the A_a and A_b transitions would explain the observation of both ClON and NO production in acetonitrile, with NO production remaining the dominant photoproduct outcome due to the preferential A_a state population.

Vibrational Lifetime. The amount of energy available to ClNO when it encounters the solvent cage depends on the rate of intermolecular vibrational relaxation. A reduction in available energy will decrease the probability of ClNO escaping the solvent cage.[43] The vibrational lifetime of ClNO appears to be solvent-dependent as evidenced by the significant increases in

ClNO vibrational line widths in acetonitrile relative to cyclohexane.[22,23] If the geminate recombination quantum yield is dependent on vibrational relaxation rate, then an increase in the relaxation rate in acetonitrile would reduce the energy available to ClNO when it encounters the solvent cage, and in turn increase the geminate recombination quantum yield.

ClNO Excited-State Evolution. Clearly, a single component of the solvent is not likely to define the photochemical quantum yields of ClNO in solution. Instead, multiple effects working in concert most likely influence which photoproducts are formed. To summarize how solvent properties affect ClNO photochemistry, we begin with a description of the reaction coordinate. Resonance Raman studies of ClNO dissolved in cyclohexane and acetonitrile demonstrate that excited-state structural evolution along the N−Cl stretch and bend coordinates occurs following A-band excitation.[22] Little to no scattering intensity was observed for the N═O stretch fundamental transition suggesting that excited-state structural evolution along this coordinate is modest. Therefore, the reaction coordinate is dominated by evolution along the N−Cl stretch as illustrated in Figure 4. As discussed above, solvent polarity alters the ground-state structure of ClNO, with the ground-state potential energy surface minimum shifting along N−Cl stretch shifting to larger bond distances in acetonitrile relative to cyclohexane.[22,23] The difference in equilibrium N−Cl bond distance impacts which excited-states are accessed following 266 nm excitation. In cyclohexane, an excited-state associated with high translational energy of the primary photoframements is accessed, while a state associated with low translational and high vibrational energy deposited into the NO photofragment is accessed in acetonitrile. As ClNO traverses the excited-state potential energy surface, it encounters a barrier to dissociation corresponding to the solvent cage. The probability of crossing this barrier is related to the barrier height (determined by the strength of the solvent cage) and the energy available to the excited ClNO (dependent on the rate of vibrational relaxation). In cyclohexane, a weak solvent cage combined with high translational energy of the photofragments results in facile cage escape. In acetonitrile, the stronger solvent cage and enhanced vibrational relaxation results in increased geminate recombination of the photofragments.

Environmental Impact. The importance of ClNO in tropospheric chemistry is linked to its abundance and ability to release Cl and NO. Until recently, ClNO was thought to be confined to marine environments where NO_2 reacts with NaCl particles from sea spray resulting in a maximum predicted mixing ratio of 0.0015 ppb in the South Coast Air Basin of California.[21] However, a new surfaced mediated ClNO formation pathway proposed by Raff et al. suggests that the tropospheric abundance of ClNO may be greater than initially thought. This new pathway involves the deposition of NO_2 onto surfaces followed by disproportionation to form $NO^+NO_3^-$, with subsequent reaction with HCl resulting in ClNO production. Molecular dynamics simulations suggest that formation of ClNO via this mechanism is enhanced by the presence of water, reaching a barrierless transition in the presence of as few as 2 water molecules.[44] The addition of this new ClNO formation pathway to climate models predicts an 8 ppb increase in ClNO mixing ratios in the South Coast Air Basin. Including gas phase photochemical properties, ClNO into the same climate model produced a 40 ppb increase in O_3, highlighting the potential impact of ClNO on our current understanding of tropospheric chemistry.

Our studies have shown that the photochemistry of ClNO is highly dependent on environment, and it is interesting to consider how this dependence might alter current climate models that employ a gas phase description of ClNO photochemistry. Specifically, gas phase models may overestimate the extent of NO and Cl production from ClNO photolysis in condensed environments. The increase in estimated ClNO mixing ratios comes as a result of the surface mediated reaction of NO_2 with HCl, considering that the photochemistry of ClNO at the air/water interface is germane in evaluating the role of ClNO in tropospheric chemical cycles. A measure of the polarity of the air/water interface is provided by second harmonic generation studies of 4-(2, 4,6-triphenylpyridinium)-2,6-diphenylphenoxide where the polarity of the air/water interface on the $E_T(30)$ polarity scale is 31.1 ± 0.07.[45] This value is remarkably close to the value of cyclohexane (30.9), suggesting that the ground-state structure of ClNO at the air/water interface should be close to that observed in cyclohexane. The similarity in polarity may also result in similar excited-state population with A-band excitation resulting in the production of Cl and NO. Molecular dynamics simulations have illustrated that the rate of vibrational relaxation decreases at interfaces relative to the bulk.[46,47] This decrease in combination with the weak solvent cage at the interface should provide for efficient Cl and NO production following ClNO photolysis. Since escape of the photofragments from the interface depends on available translational energy, the excited-states accessed by ClNO photoexcitation will play a critical role in determining the extent of Cl and NO released into the atmosphere. States characterized by high translational excitation should result in desorption of both Cl and NO. In turn, states characterized by high vibrational excitation of the NO photofragment may not have sufficient energy available to release the Cl and NO, leaving the photofragments adsorbed to the surface.

CONCLUSIONS

We have performed TRIR absorption studies of ClNO dissolved in cyclohexane, monitoring the evolution in optical density of the N═O stretch fundamental transition (ν_1) following 266 nm photoexcitation. Long-time depletion of ground-state ClNO is observed in cyclohexane following photoexcitation consistent with the absence of primary-photoproduct geminate recombination in this solvent. The evolution in optical density at frequencies corresponding to ClON and NO was measured, and an increase in optical density was observed at 1870 cm^{-1}, consistent with the production of NO. In contrast, no evidence for ClON formation was observed. These results stand in contrast to our previous studies of ClNO in acetonitrile where both geminate recombination and ClON formation were observed.

The solvent-dependence of ClNO photochemistry was discussed in terms of solvent cage strength, solvent polarity, excited-state energetics, and intermolecular vibrational relaxation, all contributing to the observed solvent-dependence. The ground-state structure of ClNO depends on solvent polarity resulting in a change in the location of the ground-state potential energy minimum along the reaction coordinate with the solvent. The solvent-dependence of the ground-state results in different excited-states being accessed following 266 nm photoexcitation. This combined with the presence of a stronger

solvent cage in acetonitrile is largely responsible for the differences of ClNO photochemistry observed between acetonitrile and cyclohexane.

AUTHOR INFORMATION

Corresponding Author

*E-mail: preid@chem.washington.edu.

Notes

The authors declare no competing financial interest.

ACKNOWLEDGMENTS

The National Science Foundation (CHE-0350191) is acknowledged for their support of this work. We would like to acknowledge the work of Jane Schultz in the initial preparation of the experimental apparatus and molar extinction coefficient measurements.

REFERENCES

(1) Vaida, V. *J. Chem. Phys.* **2011**, *135*, 020901.
(2) Cooksey, C. C.; Reid, P. J. *Photochem. Photobiol.* **2004**, *80*, 386.
(3) Reid, P. J. *J. Phys. Chem. A* **2002**, *106*, 1473.
(4) Vaida, V.; Simon, J. D. *Science* **1995**, *268*, 1443.
(5) Arkell, A.; Schwager, I. *J. Am. Chem. Soc.* **1967**, *89*, 5999.
(6) Holger, S.; Mueller, P.; Willner, H. *J. Phys. Chem.* **1993**, *97*, 10589.
(7) Rochkind, M. M.; Pimentel, G. C. *J. Chem. Phys.* **1967**, *46*, 4481.
(8) Hayes, S. C.; Philpott, M. J.; Reid, P. J. *J. Chem. Phys.* **1998**, *109*, 2596.
(9) Hayes, S. C.; Philpott, M. P.; Mayer, S. G.; Reid, P. J. *J. Phys. Chem. A* **1999**, *103*, 5534.
(10) Hayes, S. C.; Thomsen, C. L.; Reid, P. J. *J. Chem. Phys.* **2001**, *115*, 11228.
(11) Philpott, M. J.; Charalambous, S.; Reid, P. J. *Chem. Phys. Lett.* **1997**, *281*, 1.
(12) Philpott, M. J.; Hayes, S. C.; Reid, P. J. *Chem. Phys.* **1998**, *236*, 207.
(13) Philpott, M. J.; Hayes, S. C.; Thomsen, C. L.; Reid, P. J. *Chem. Phys.* **2001**, *263*, 389.
(14) Poulsen, J. A.; Thomsen, C. L.; Keiding, S. R.; Thogersen, J. *J. Chem. Phys.* **1998**, *108*, 8461.
(15) Thogersen, J.; Jepsen, P. U.; Thomsen, C. L.; Poulsen, J. A.; Byberg, J. R.; Keiding, S. R. *J. Phys. Chem. A* **1997**, *101*, 3317.
(16) Thogersen, J.; Thomsen, C. L.; Poulsen, J. A.; Keiding, S. R. *J. Phys. Chem. A* **1998**, *102*, 4186.
(17) Thomsen, C. L.; Philpott, M. P.; Hayes, S. C.; Reid, P. J. *J. Chem. Phys.* **2000**, *112*, 505.
(18) Thomsen, C. L.; Reid, P. J.; Kieding, S. R. *J. Am. Chem. Soc.* **2000**, *122*, 12795.
(19) Bolinger, J. C.; Bixby, T. J.; Reid, P. J. *J. Chem. Phys.* **2005**, *123*, 084503.
(20) Finlayon-Pitts, B. J.; Pitts, J. N. *Chemistry in the Upper and Lower Atmosphere*; Academic Press: New York, 2000.
(21) Raff, J. D.; Njegic, B.; Chang, W. L.; Gordon, M. S.; Dabdub, D.; Gerber, R. B.; Finlayson-Pitts, B. J. *Proc. Natl. Acad. Sci. U.S.A.* **2009**, *106*, 13647.
(22) Nyholm, B. P.; Reid, P. J. *J. Phys. Chem. B* **2004**, *108*, 8716.
(23) Bixby, T. J.; Patterson, J. D.; Reid, P. J. *J. Phys. Chem. A* **2009**, *113*, 3886.
(24) Cooksey, C. C.; Johnson, K. J.; Reid, P. J. *J. Phys. Chem. A* **2006**, *110*, 8613.
(25) Pass, G.; Sutcliffe, H. *Practical Inorganic Chemistry: Preparation, Reactions, and Instrumental Methods*; Chapman and Hall: London, U.K., 1968.
(26) Hallou, A.; Schriver-Mazzuoli, L.; Schriver, A.; Chaquin, P. *Chem. Phys.* **1998**, *237*, 251.
(27) Maier, G.; Reisenauer, H. P.; De Marco, M. *Chem.—Eur. J.* **2000**, *6*, 800.
(28) Fateley, W. G.; Bent, H. A.; Crawford, B. Jr. *J. Chem. Phys.* **1959**, *31*, 204.
(29) Krim, L.; Lacome, N. *J. Phys. Chem. A* **1998**, *102*, 2289.
(30) Lynch, M. S.; Cheng, M.; Van Kuiken, B. E.; Khalil, M. *J. Am. Chem. Soc.* **2001**, *133*, 5255.
(31) Noyes, R. M. *J. Am. Chem. Soc.* **1955**, *77*, 2042.
(32) Bunker, D. L.; Jacobson, B. S. *J. Am. Chem. Soc.* **1972**, *94*, 1843.
(33) Nesbitt, D. J.; Hynes, J. T. *J. Chem. Phys.* **1982**, *77*, 2130.
(34) Harris, A. L.; Brown, J. K.; Harris, C. B. *Annu. Rev. Phys. Chem.* **1988**, *39*, 341.
(35) Meredith, C.; Quelch, G. E.; Schaeffer, H. F. *J. Chem. Phys.* **1992**, *96*, 480.
(36) Basco, N.; Norrish, R. G. W. *Proc. R. Soc. Lond. A* **1962**, *268*, 291.
(37) Werner, L.; Wunderer, B.; Walther, H. *Chem. Phys.* **1981**, *60*, 109.
(38) Moser, M. D.; Weitz, E.; Schatz, G. C. *J. Chem. Phys.* **1983**, *78*, 757.
(39) Haas, B. M.; Felder, P.; Huber, J. R. *Chem. Phys. Lett.* **1991**, *180*, 293.
(40) Kim, H. L.; Mo, Y.; Matsumi, Y.; Kawasaki, M. *Bull. Korean Chem. Soc.* **1992**, *13*, 162.
(41) Felder, P.; Morley, G. P. *Chem. Phys.* **1994**, *185*, 145.
(42) Skorokhodov, V.; Sato, Y.; Suto, K.; Matsumi, Y.; Kawasaki, M. *J. Phys. Chem.* **1996**, *100*, 12321.
(43) Chorny, I.; Vieceli, J.; Benjamin, I. *J. Chem. Phys.* **2002**, *116*, 8930.
(44) Njegic, B.; Raff, J. D.; Finlayson-Pitts, B. J.; Gordon, M. S.; Gerber, R. B. *J. Phys. Chem. A* **2010**, *114*, 4609.
(45) Wang, H. F.; Borguet, E.; Eisenthal, K. B. *J. Phys. Chem. B* **1998**, *102*, 4927.
(46) Benjamin, I. *J. Phys. Chem. B* **2006**, *110*, 9375.
(47) Chorny, I.; Vieceli, J.; Benjamin, I. *J. Phys. Chem. B* **2003**, *107*, 229.